High performance CNT point emitter with graphene interfacial layer

2014 Nanotechnology 25 455601

(http://iopscience.iop.org/0957-4484/25/45/455601)

IOP Publishing Nanotechnology
Nanotechnology 25 (2014) 455601 (8pp) doi:10.1088/0957-4484/25/45/455601

High performance CNT point emitter with graphene interfacial layer

Jeong Seok Lee[1], Taewoo Kim[1], Seul-Gi Kim[3], Myung Rae Cho[4], Dong Kyun Seo[1], Minwoo Lee[5], Seontae Kim[4], Dae Weon Kim[6], Gun-Sik Park[4], Dae Hong Jeong[5], Yun Daniel Park[4], Ji-Beom Yoo[3], Tae June Kang[2] and Yong Hyup Kim[1]

[1] School of Mechanical and Aerospace Engineering, Seoul National University, Seoul 151-742, Korea
[2] Department of NanoMechatronics Engineering and BK21 Plus Nano Convergence Technology Division, College of Nanoscience and Nanotechnology, Pusan National University, Busan 609-735, Korea
[3] School of Advanced Materials Science & Engineering, Sungkyunkwan University, Gyeonggi-do 440-746, Korea
[4] Department of Physics & Astronomy, Seoul National University, Seoul 151-742, Korea
[5] Department of Chemistry Education, Seoul National University, Seoul 151-742, Korea
[6] Department of Naval Architecture, Kunsan National University, Gunsan 573-701, Korea

E-mail: tjkang@pusan.ac.kr and yongkim@snu.ac.kr

Received 25 June 2014, revised 18 August 2014
Accepted for publication 22 September 2014
Published 20 October 2014

Abstract

Carbon nanotubes (CNTs) have great potential in the development of high-power electron beam sources. However, for such a high-performance electronic device, the electric and thermal contact problem between the metal and CNTs must be improved. Here, we report graphene as an interfacial layer between the metal and CNTs to improve the interfacial contact. The interfacial graphene layer results in a dramatic decrease of the electrical contact resistance by an order of 2 and an increase of the interfacial thermal conductivity by 16%. Such a high improvement in the electrical and thermal interface leads to superior field emission performance with a very low turn-on field of 1.49 V μm^{-1} at 10 $\mu A\ cm^{-2}$ and a threshold field of 2.00 V μm^{-1} at 10 mA cm^{-2}, as well as the maximum current of 16 mA (current density of 2300 A cm^{-2}).

Keywords: graphene, carbon nanotube, interfacial layer, field emission, point emitter

(Some figures may appear in colour only in the online journal)

1. Introduction

By taking advantage of the superior material properties and high aspect ratio geometry of CNTs [1], many researchers have been able to devote their efforts toward the development of CNT point emitters, which are capable of providing low turn-on voltage, high emission current density and long-term emission stability [2–6]. The extremely high current density of the point emitter plays an essential role as a sufficient power source in microwave amplifier tubes, high-resolution electron-beam instruments and x-ray sources [7].

A CNT point emitter generally has the configuration of a one-dimensional CNT structure at a conductive metal tip. The adhesion method of CNTs at a metal tip is appropriate for the fabrication of the point emitter when considering the quality issues of CNTs in the growth method [8, 9]. The CNT point emitters, based on the adhesion method, were fabricated either by the wet-spinning of CNT fibers [10], the crystal-like growth method [11] or by attaching CNTs using dielectrophoresis [12], utilizing well-dispersed CNT colloidal solutions. However, these methods usually result in emitters with high thermal and electrical contact resistances between the metal and CNT, which seriously degrade the field emission performances of the emitters [13–15]. A high electrical contact resistance not only increases the electric field for electron emissions but also causes electrical Joule heating at the contact interface. High thermal contact resistance frequently decreases the lifetime of the emitter due to the sublimation of CNTs [16, 17].

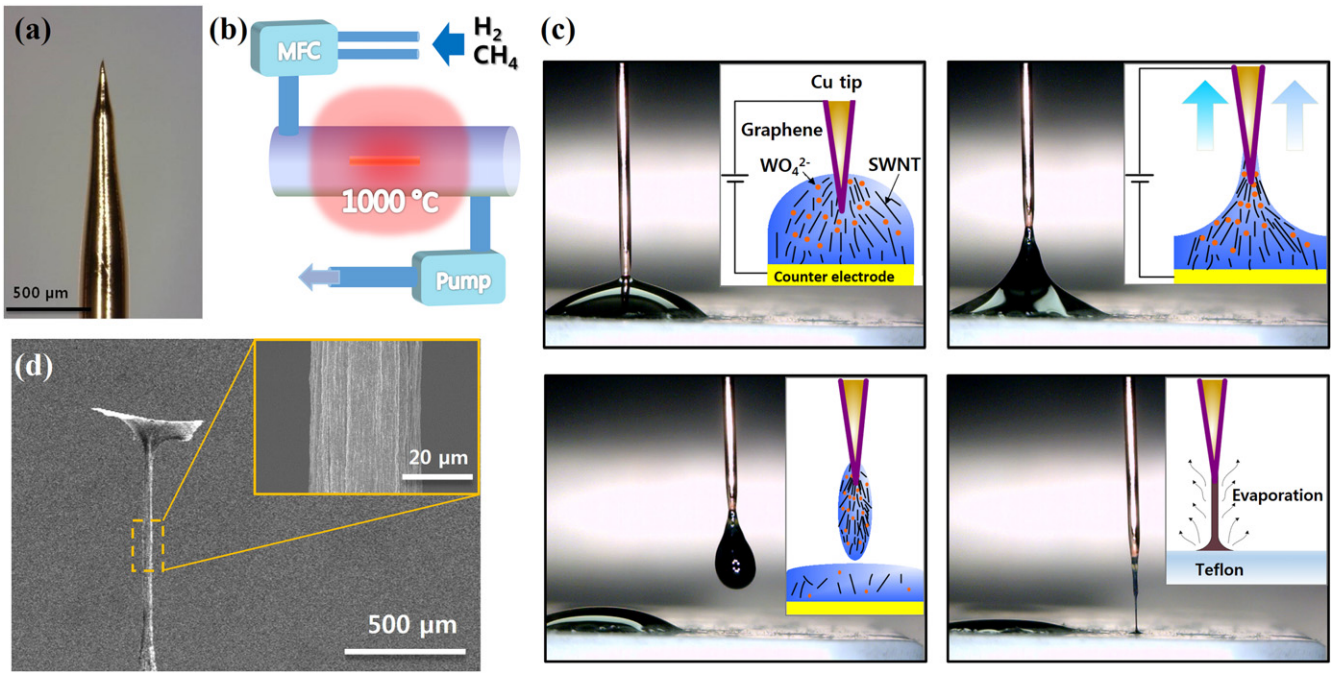

Figure 1. (a) An optical image of sharpened copper wire using the electro-chemical etching process. (b) Schematic drawing to fabricate the graphene growth by chemical vapor deposition (CVD). (c) Optical images of a carbon nanotube point emitter through the crystal-like growth method. (Inset shows the schematic drawing of the crystal-like growth method.) (d) Scanning electron micrograph of the point emitter that is comprised of an aligned carbon nanotube with one direction.

Various efforts have been devoted to improving the electric and thermal interfaces between metal and CNTs. These efforts include metal welding to CNTs using an ultrasonic bonder [18], an additional carbon layer deposition using EBID (electron beam-induced deposition) [19] and depositing a graphitic layer via heat treatment at a temperature above 880 K [20]. Various methods [21, 22], in addition to those mentioned above, could reduce the electrical contact resistance by an order of 1 to 3; however, no attempt was made at reducing the thermal resistance. In addition, these methods usually require a high temperature process or additional cumbersome treatments. A simple and effective method to improve the interface between metal and CNTs is necessary.

In the present study, we have investigated graphene as an interfacial layer between metal and CNTs to improve the interfacial contact properties. Single-layer graphene has remarkable electron mobility (~150 000 $cm^2\ Vs^{-1}$) and thermal conductivity (~3100–5300 $W\ mK^{-1}$) [23, 24]. Moreover, since graphene is a two-dimensional material and basically consists of the same atomic structure as CNT, exhibiting a similar work function of ~4.5 eV [25, 26], graphene has great potential in the interfacial layer to improve the electric and thermal interfaces between metal surface and CNTs. By adopting graphene to the interfacial layer between metals and CNTs, we successfully achieved a dramatic decrease of the electrical contact resistance by an order of 2 and an increase of the thermal conductivity by 16%. The performance of the CNT point emitter, including the graphene interfacial layer, is also greatly improved.

2. Methods

2.1. Crystal-like growth of the metal oxide/CNT composite fiber

The copper tip is submerged in n,n-DMF solution, which consists of CNT and sodium tungstate; then, an electric current of 1 mA is applied. Due to the applied bias between the copper tip and counter electrode, negatively charged CNTs gather around the copper tip with WO_4^{2-}. After being submerged for 5 min, the copper tip is extracted, and a droplet, which includes the CNT and WO_3 composite, is formed at the end of the copper tip. The droplet is in the form of a gel and is moved to have a contact with the Teflon surface, resulting in a vertically aligned one-dimensional composite structure after the drying process.

2.2. Instruments and methods

The field emission characteristics were measured at room temperature under 3×10^{-7} torr. A voltage between the CNT cathode and an anode was applied using a DC power supply (Matsusade Precision Inc.). The plate-shaped molybdenum (Mo) was used as the anode. The emission current was measured using a multimeter (Keithley 2000). The distance between the cathode and anode was fixed at 500 μm by a separator. SEM analysis was performed using a Hitachi S-4800 field-emission electron microscope at an acceleration voltage of 10–15 KeV. Raman spectra were obtained using a micro Raman system (Horiba Jobin-Yvon LabRAM 300) with a 50X objective lens (Olympus, NA 0.75).

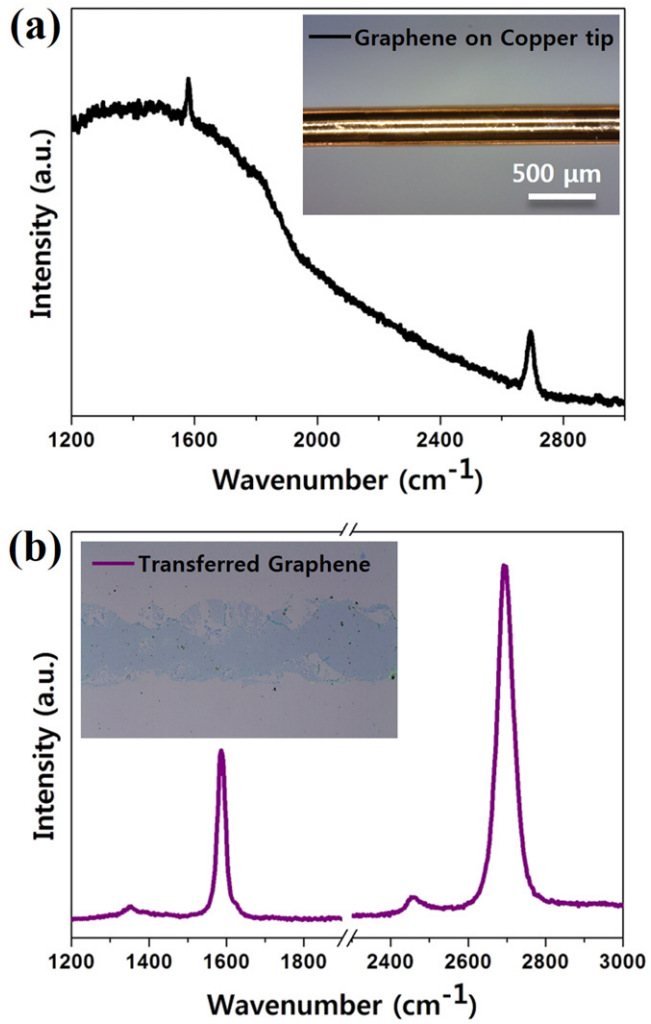

Figure 2. (a) Raman spectrum of graphene on a copper tip obtained by 532 nm photoexcitation. (Inset shows an optical image of the copper wire after graphene growth.) (b) Raman spectrum of the transferred graphene on the silicon substrate obtained by 532 nm photoexcitation. (Inset shows an optical image of the transferred graphene to the silicon substrate.)

3. Results and discussion

A CNT point emitter was fabricated by the crystal-like growth method [11, 27] using a copper wire tip, as shown in figure 1. The tip of the copper wire was sharpened by electro-chemical etching [28] (figure 1(a)), followed by a graphene synthesis on the wire using the CVD process with H_2 and CH_4 gas flows at 1000 °C (figure 1(b)) [29]. Figure 1(c) shows the experimental procedure used to fabricate the CNT point emitter based on a single-walled CNT (SWNT) colloidal solution mixed with sodium tungstate (see the methods section in the supporting information for details) [11]. The SWNTs have a length of 5–10 μm, and the average bundle diameter of the SWNTs is determined from transmission electron microscopy (TEM) analysis as 7 nm (figure S1 in the supporting information). Upon applying the bias between the copper tip and counter electrode, the CNTs that are negatively charged through the purification process and the WO_4^{2-} migrate to the copper tip. The WO_4^{2-} changes into WO_3 during the plating process, encouraging tight contact between the adjacent CNTs as well as the CNT and the graphene surface. An electron probe microanalysis (EPMA) technique reveals that the tungsten and carbon are uniformly distributed throughout the composite structure in which the WO_3 was electroplated on the SWNT wall [11]. After the electroplating process, the copper tip is withdrawn with a droplet; the CNT and WO_3 composite are included. The droplet is placed on a Teflon surface to constrain the free end of droplet, resulting in a straight one-dimensional composite structure after solvent evaporation.

The composite structure is finally detached from the Teflon surface, as shown in figure 1(d); then, the resulting emitter has a cylindrical geometry with a diameter of ~30 μm, of which the length can be controlled by adjusting the plating time [11]. The 'nail head' geometry (see the tip of the CNT emitter in figure 1(d)) is formed due to the contact-drying process that is necessary to make the structure straight. The nail head can be removed by a post-processing treatment. As shown in the inset of figure 1(d), the CNTs are well aligned along the emitter axis. The CNTs, which are randomly dispersed in the solution, are aligned in the direction of the emitter during the crystal-like growth process [11]. Since the alignment is made in the direction of the electron path during the field emission, the self-alignment helps to enhance the performances of the emitter.

Ensuring that the high-quality graphene is uniformly synthesized on the surface of the copper wire before the crystal-like growth of the CNT emitter is the most important step in the present study. The inset of figure 2(a) shows the optical image of the copper wire after the synthesis of the graphene layer. To confirm a graphene layer on the copper wire, Raman analysis was carried out, as shown in figure 2(a). The Raman peaks, characteristic of the G-band (~1579 cm^{-1}) and 2D-band (~2693 cm^{-1}) of the graphene, are clearly observed over a broad background signal of the copper. Almost identical Raman characteristics were observed along the lengthwise direction of the Cu wire and along the cone-shaped region, confirming the uniform growth of graphene on the wire (figure S2 in the supporting information). We transferred the graphene onto a silicon substrate to exclusively analyze the characteristics. The inset of figure 2(b) shows the optical image of the graphene transferred to a silicon substrate after etching the copper wire and drying it at an ambient condition. The cylindrical structure of the graphene that wrapped around the copper wire collapsed into a ribbon geometry during the transfer process. The Raman spectra of the transferred graphene are shown in figure 2(b). The intensity of the D-band at ~1350 cm^{-1} is negligible, and the 2D/G ratio was estimated to be ~2.1, indicating that one or two layers of high-quality graphene was successfully synthesized on the copper wire [30]. An atomic force microscopy (AFM) study also revealed a thickness of ~1 nm for the graphene layer, as determined by the Raman analysis (figure S3 in the supporting information).

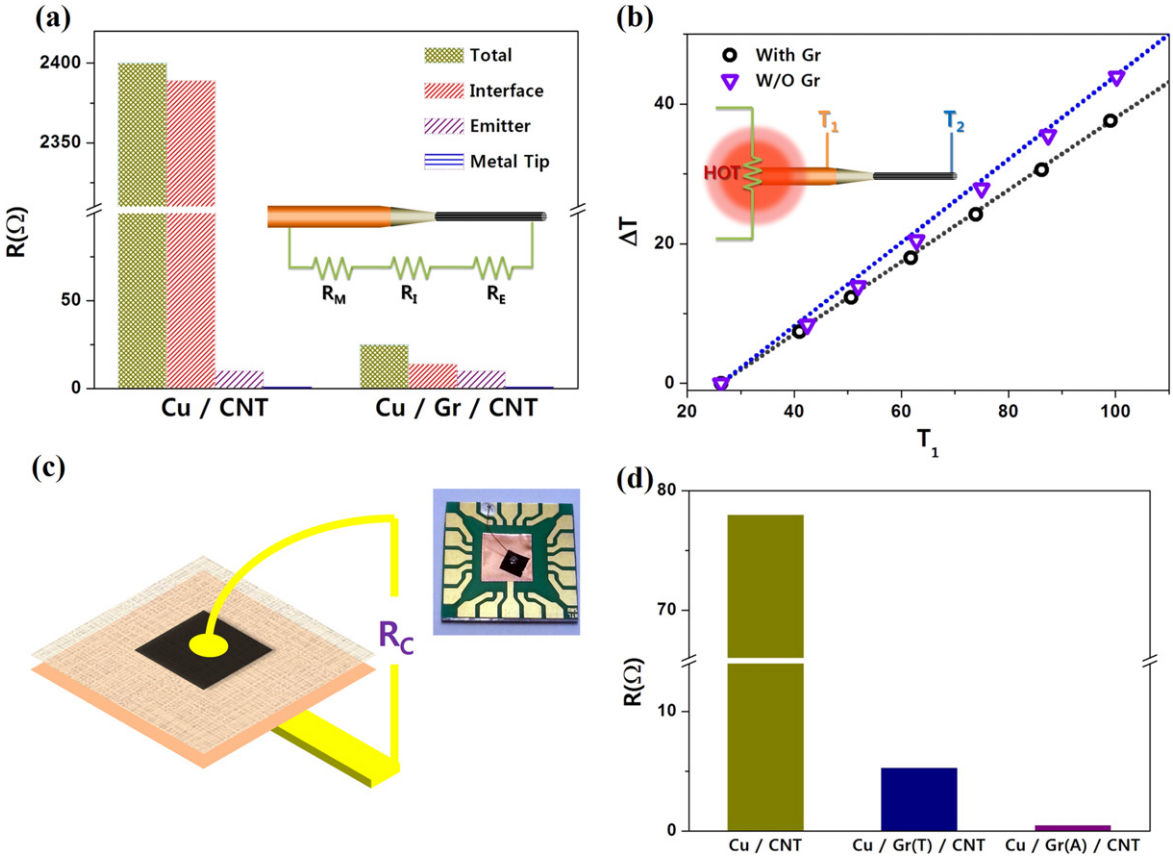

Figure 3. (a) Graph shows the change of resistance due to the graphene interfacial layer. (Inset shows three electrical resistance components: R_M is the resistance of copper wire, R_I is the interface resistance and R_E is the resistance of the point emitter.) (b) Graph shows the improvement of the heat conductivity by 16% with the graphene interfacial layer. (Inset shows schematic drawings of the thermal conductivity measurement.) (c) Schematic drawing and optical image to measure the electrical contact resistance. (d) Comparison of the contact resistance between the copper and CNT with and without a graphene layer (Gr(T) is the transferred graphene layer and Gr(A) is the as-grown graphene layer.)

The effectiveness of the graphene interfacial layer for electrical and thermal contacts was demonstrated, as shown in figure 3. The total electrical resistance of the CNT point emitter consists of the resistances of the copper wire, the CNT structure and the interfacial contact resistance between the copper tip and the CNTs, as schematically described in the inset of figure 3(a). The contact resistance was evaluated by subtracting the resistances of the copper wire and the CNT structure from the total resistance of the emitter. The contact resistance of the emitter without graphene was 2.39 kΩ, which corresponds to most of the total resistance (2.40 kΩ), while the emitter with the graphene interfacial layer shows 25 Ω of the total resistance, having a very low contact resistance of 14 Ω. It is noteworthy that the contact resistance of the emitter with the graphene interfacial layer is 2 orders of magnitude lower than that without the layer.

Since the field emission stability of a CNT emitter is degraded by the sublimation of the CNTs at the end of the emitter, the high thermal conductivity of the emitter is very important so that it rapidly dissipates the heat generated during emission. The thermal interfacial resistance of the present emitter was investigated by comparing the thermal conductivity of the emitter with and without a graphene interfacial layer, as shown in figure 3(b). The emitters with and without a graphene interfacial layer prepared with the same geometry (i.e. the emitter length and diameter) were placed in a vacuum chamber ($\sim 10^{-3}$ torr) to minimize the heat convection effect of air. The controlled temperature was applied to the end of the copper wire using electrical Joule heating of the chromium wire (see the inset of figure 3(b)). The temperatures of the copper wire (T_1) and the CNT emitter tip (T_2) were measured using a thermocouple by making a contact with thermally conductive epoxy. Figure 3(b) shows the temperature differences ($\Delta T = T_1 - T_2$) with respect to the applied temperature to the copper wire. The thermal conductivity ratio can be expressed as the inverse of the temperature change ratio ($K_w/K_{w/o} = \Delta T_{w/o}/\Delta T_w$) based on the heat conduction equation, where K represents the thermal conductivity, and the subscripts w and w/o denote the samples with and without a graphene interfacial layer, respectively. The temperature change shows a linear relationship with respect to the applied temperature. It is noteworthy that the use of a graphene interfacial layer increases the thermal conductivity of the emitter by 16%, as shown in figure 3(b).

In metals with poor wettability, such as Pt, Ni, Ag and Cu, the contact barrier (such as a vacuum gap or surface oxides) is

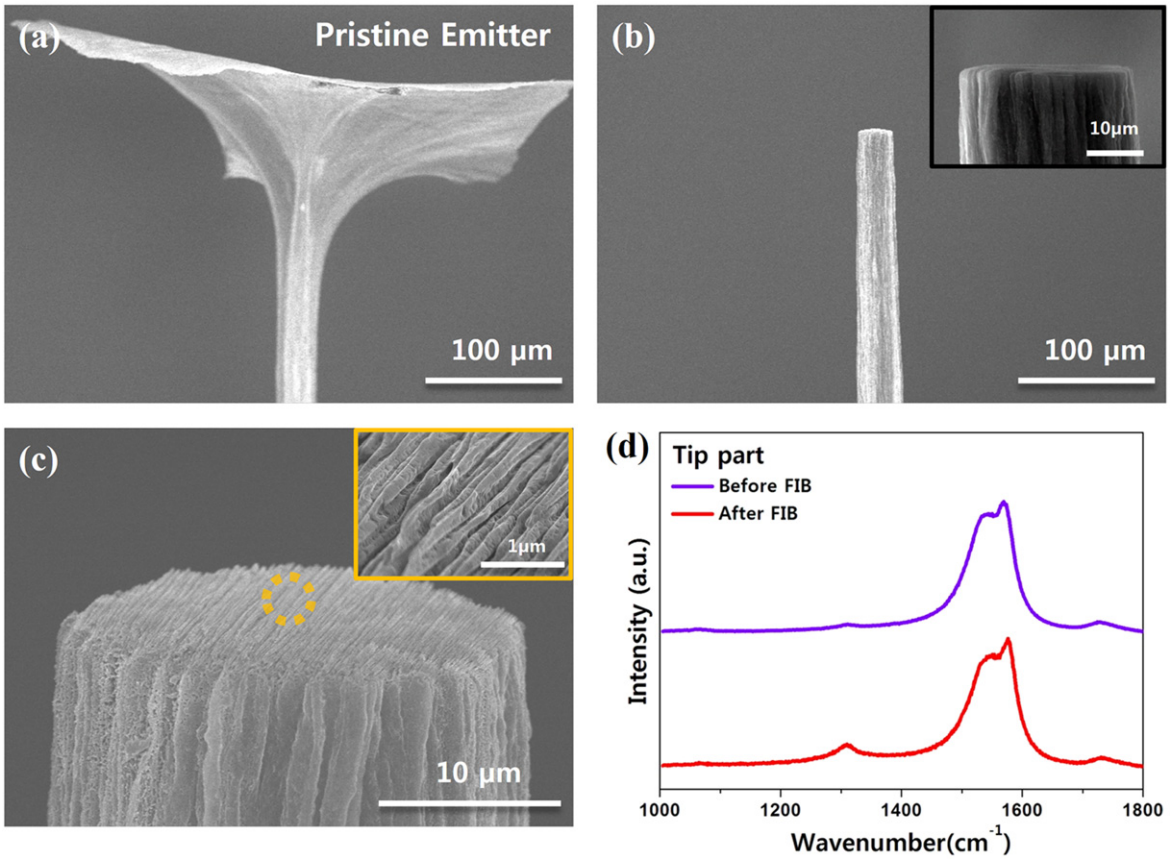

Figure 4. (a) Scanning electron micrograph of the pristine emitter with the nail head. (b) Scanning electron micrograph of the emitter with the nail head removed by FIB treatment. (c) The close-up scanning electron micrograph of the cross-section area with the FIB treatment. Inset image shows the trace of the Ga ion during the FIB treatment. (d) Raman spectra obtained by 532 nm photoexcitation at the cross-section area of the carbon nanotube point emitter of the two cases before FIB and after FIB treatment.

easily formed between the metal and the CNT [31]. van der Waals force is not great enough to make complete physical contact between the copper and the CNT, as previously observed in the dewetting phenomena of CNTs and metal contacts [32, 33] in which an atomic-level vacuum gap was observed. The atomic-level vacuum gap results in large electrical contact resistance [34]. However, if we prepare copper with the surface covered by a synthesized graphene layer through carbon segregation and/or a precipitation process, the graphene automatically has maximized contact area with the copper. Moreover, the graphene has not only ohmic contact with the CNT because of an almost identical work function but also a large contact area with the CNT due to the van der Waals forces and to π–π stacking interactions [35, 36]. As a consequence, the adoption of the graphene interfacial layer results in very low contact resistance of the emitter.

To confirm the effect of the contact area between the copper and CNTs, we prepared three specimens with different stacking sequences: (1) copper and CNTs; (2) copper, transferred graphene and CNTs; and (3) copper with synthesized graphene and CNTs. We measured their electrical contact resistance, as shown in figures 3((c)–(d)). The CNT layer is simply stacked by placing a thin CNT film on the specimens. The contact resistance between the copper and the CNT with the synthesized graphene interfacial layer is 150 times lower than that without the graphene layer and 10 times lower than that with the transferred graphene interfacial layer. The lower contact resistance with the graphene layer than without the graphene layer could be attributed to the increased contact area and the π–π stacking interactions due to the graphene interfacial layer. Moreover, it is clear that the synthesized graphene interfacial layer allows a larger contact area between the copper and graphene than the transferred graphene layer. It is believed that metal-based contamination or wrinkles that occurred during the wet transfer process adopted in this test causes a physical gap between the copper and the transferred graphene layer [37, 38].

The improved interface with the graphene layer may enhance the field emission performance of the present emitter. The effect of adopting the graphene layer to the emitter was investigated with respect to the field emission performance. The nail head geometry of the emitter tip, shown in figure 1(d), results from a pinning effect and from the capillary flow in which the contact line of the drying column on the Teflon surface is replenished by solvent from the interior as the solvent evaporates from the edge. The nail head geometry at the tip of the emitter is not desirable for a point emitter because it degrades the electric field concentration and structural robustness. An EDM (electric discharge machining) process could be utilized to remove the nail head [27].

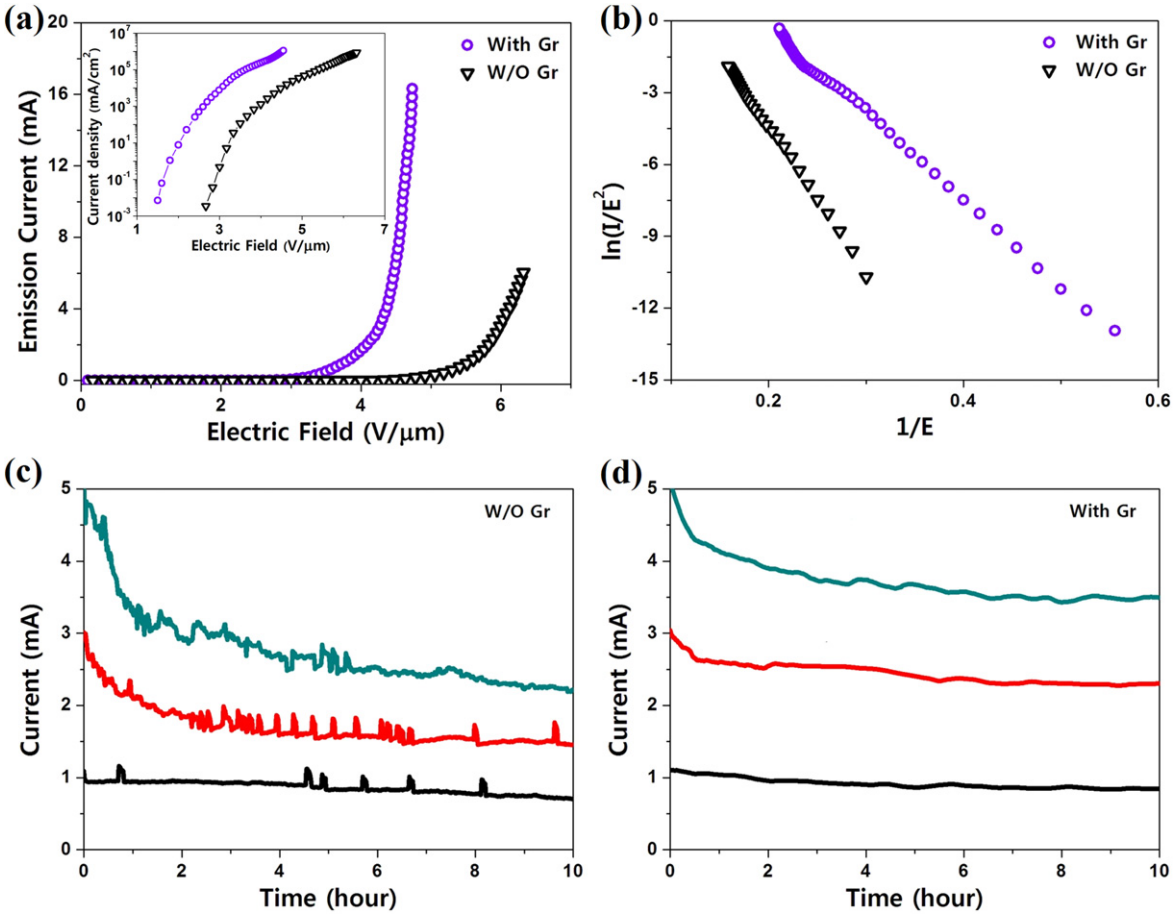

Figure 5. (a) I-V plots of the point emitter with and without the graphene interfacial layer. (Inset shows the J-E plot with the logarithmic current density.) (b) Fowler–Nordheim plots of field emission characteristics (I-V plot). ((c), (d)) Field emission stability test of the emitter without and with the graphene interfacial layer.

However, a very high current (~7 ampere) that passed through the CNT emitter might degrade the electrical properties of CNT emitter. Thus, we adopted a focused ion beam (FIB) treatment to remove the nail head. It was severed from the emitter by the irradiation of the Ga ion beam with high energy. The emitter without the nail head is clearly shown in the SEM image of figure 4(b) and has a diameter of 30 μm. From the SEM observation of figure 4(c), the severed surface is formed in a very consistent and regular manner and textured in the direction of beam irradiation. Raman analysis was carried out to investigate the effect of the FIB treatment on the surface of the CNT emitter tip. In the Raman spectra of the emitter before and after the FIB treatment, the change of G/D ratio is insignificant. The slight increase of the D peak could be attributed to physical damage on the CNT due to Ga ion collisions.

Figure 5 shows the field emission characteristics of the CNT point emitters. The distance between the cathode tip and anode (d) was used to calculate the macroscopic field ($E = V/d$, where E and V represent an applied electric field and the voltage) [4]. It is noteworthy, as shown in figure 5(a), that the turn-on field (E_{on}: 1.49 V μm^{-1} at 10 μA cm^{-2}) and the threshold field (E_{th}: 2.00 V μm^{-1} at 10 mA cm^{-2}) of the emitter with the graphene interfacial layer are considerably lower than those without the graphene interface (E_{on}: 2.74 V μm^{-1}, E_{th}: 3.25 V μm^{-1}). Moreover, the maximum current of the emitter with the graphene interfacial layer reaches up to 16 mA, which corresponds to the current density of 2300 A cm^{-2}, while it is 6 mA for the emitter without the graphene interface. It is obvious that the improved electrical and thermal contacts between the copper wire and the CNT emitter are responsible for the enhancement of the emission performance. Figure 5(b) shows the Fowler–Nordheim (F–N) curves of the emission, and the slope of the F–N curve represents the field enhancement factor of an emitter. The field enhancement factor of 2120 for the emitter with the graphene interfacial layer is almost two times higher than that of 1180 for the emitter without a graphene interface. The CNT emitter with high electrical and thermal conductivity is attributed to the excellent field emission characteristics. Moreover, it is interesting that two distinct behaviors regarding the F–N curves were observed. The field enhancement factor of the emitters with and without a graphene interface is almost linear in a low field region. However, it turns nonlinear in the region of the high electrical field because of the thermally enhanced electron emission due to Joule heating of the carbon nanotube [39]. Joule heating at the tip of the emitter, which may exceed up to 1000 K, adds a

thermionic emission current to the field emission, enhancing the overall emission performance [40].

The emission stability of the present emitter was investigated by a continuously performing emission with a current of 1–5 mA for 10 h, as shown in figures 5(c) and (d). The current is not stable during the test in the emitter without a graphene interface, and considerable degradation was observed, for instance, 30% in 1 mA, 50% in 3 mA and 56% in 5 mA after 10 h of operation (figure 5(c)). As shown in figures 3(a) and (b), the emitter without the graphene layer has high electrical and thermal resistance, especially at the interface. At a given field emission current for the stability tests, the emitter without a graphene layer demands a higher electric field compared to that of the emitter with the graphene layer, which in turn leads to severe heat accumulation. It might lead to the oxidation and/or the severe degradation of the emitters by Joule heating [41]. However, the emission stability was significantly improved when the emitter with the graphene interfacial layer was used, as shown in figure 5(d). The reasonably small degradation in the current was observed after 10 h of operation to be 15% in 1 mA, 23% in 3 mA and 30% in 5 mA.

4. Conclusion

The contact interface involved in fabricating a CNT point emitter is one of the important issues to be resolved. In the present study, the adoption of graphene as an interfacial layer between the metal and the CNT has been investigated. High-quality graphene was uniformly grown on a copper wire. The interfacial graphene layer results in a dramatic decrease of the electrical contact resistance by an order of 2 and an increase of the interfacial thermal conductivity by 16%. Such a high improvement in the electrical and thermal interface leads to the superior field emission performance with a very low turn-on field of 1.49 V μm^{-1} at 10 $\mu A\ cm^{-2}$ and a threshold field of 2.00 V μm^{-1} at 10 mA cm^{-2}, as well as the maximum current of 16 mA (current density of 2300 A cm^{-2}). The emitter also shows stable emission characteristics with a high current of 5 mA (700 A cm^{-2}) for 10 h.

Acknowledgments

This research was supported by the National Research Foundation of Korea (Grant nos. 2009-0083512, 2011-0024818, 2014R1A2A1A05007760 and 2014R1A1A4A01008768); the Defense Acquisition Program Administration and Agency for Defense Development under Contract UD100048JD; Pusan National University Research Grant 2012; the Civil & Military Technology Cooperation Program through the National Research Foundation of Korea (NRF), funded by the Ministry of Science; ICT & Future Planning (No. 2013M3C1A9055407); and the Brain Korea 21 Plus Project in 2014. The authors also acknowledge support from the Institute of Advanced Aerospace Technology at Seoul National University.

References

[1] Baughman R H, Zakhidov A A and de Heer W A 2002 Carbon nanotubes–the route toward applications *Science* **297** 787–92
[2] Minoux E *et al* 2005 Achieving high-current carbon nanotube emitters *Nano Lett.* **5** 2135–8
[3] Zhu L, Sun Y, Hess D W and Wong C-P 2006 Well-aligned open-ended carbon nanotube architectures: an approach for device assembly *Nano Lett.* **6** 243–7
[4] Perea-López N *et al* 2011 Millimeter-long carbon nanotubes: outstanding electron-emitting sources *ACS Nano* **5** 5072–7
[5] Liu P, Wei Y, Liu K, Liu L, Jiang K and Fan S 2012 New-type planar field emission display with superaligned carbon nanotube yarn emitter *Nano Lett.* **12** 2391–6
[6] Yuge R, Miyawaki J, Ichihashi T, Kuroshima S, Yoshitake T, Ohkawa T, Aoki Y, Iijima S and Yudasaka M 2010 Highly efficient field emission from carbon nanotube–nanohorn hybrids prepared by chemical vapor deposition *ACS Nano* **4** 7337–43
[7] Sugie H, Tanemura M, Filip V, Iwata K, Takahashi K and Okuyama F 2001 Carbon nanotubes as electron source in an x-ray tube *Appl. Phys. Lett.* **78** 2578–80
[8] Ferrer D, Tanii T, Matsuya I, Zhong G, Okamoto S, Kawarada H, Shinada T and Ohdomari I 2006 Enhancement of field emission characteristics of tungsten emitters by single-walled carbon nanotube modification *Appl. Phys. Lett.* **88** 033116
[9] Chen G, Shin D H, Roth S and Lee C J 2009 Field emission characteristics of point emitters fabricated by a multiwalled carbon nanotube yarn *Nanotechnology* **20** 315201
[10] Zhang S, Koziol K K K, Kinloch I A and Windle A H 2008 Macroscopic fibers of well-aligned carbon nanotubes by wet spinning *Small* **4** 1217–22
[11] Kim W J, Jang E Y, Seo D K, Kang T J, Jin K C, Jeong D H and Kim Y H 2010 Crystal-like growth of a metal oxide/CNT composite fiber with electroplated 'seed' from a CNT-dispersed nonaqueous electrolyte *Langmuir* **26** 15701–5
[12] Jung S I, Choi J S, Shim H C, Kim S, Jo S H and Lee C J 2006 Fabrication of probe-typed carbon nanotube point emitters *Appl. Phys. Lett.* **89** 233108
[13] Liu N, Fang G, Zeng W, Zhou H, Long H and Zhao X 2012 Enhanced field emission from three-dimensional patterned carbon nanotube arrays grown on flexible carbon cloth *J. Mater. Chem.* **22** 3478–84
[14] Das S, Seelaboyina R, Verma V, Lahiri I, Hwang J Y, Banerjee R and Choi W 2011 Synthesis and characterization of self-organized multilayered graphene-carbon nanotube hybrid films *J. Mater. Chem.* **21** 7289–95
[15] Wu C, Li F, Zhang Y and Guo T 2012 Improving the field emission of graphene by depositing zinc oxide nanorods on its surface *Carbon* **50** 3622–6
[16] Deng J-H, Zheng R-T, Zhao Y and Cheng G-A 2012 Vapor–solid growth of few-layer graphene using radio frequency sputtering deposition and its application on field emission *ACS Nano* **6** 3727–33
[17] Neupane S, Lastres M, Chiarella M, Li W, Su Q and Du G 2012 Synthesis and field emission properties of vertically aligned carbon nanotube arrays on copper *Carbon* **50** 2641–50
[18] Chen C, Liu L, Lu Y, Kong E S-W, Zhang Y, Sheng X and Ding H 2007 A method for creating reliable and low-resistance contacts between carbon nanotubes and microelectrodes *Carbon* **45** 436–42
[19] Rykaczewski K, Henry M R, Kim S-K, Fedorov A G, Kulkarni D, Singamaneni S and Tsukruk V V 2010 The effect of the geometry and material properties of a carbon

joint produced by electron beam induced deposition on the electrical resistance of a multiwalled carbon nanotube-to-metal contact interface *Nanotechnology* **21** 035202
[20] Kane A A, Sheps T, Branigan E T, Apkarian V A, Cheng M H, Hemminger J C, Hunt S R and Collins P G 2009 Graphitic electrical contacts to metallic single-walled carbon nanotubes using pt electrodes *Nano Lett.* **9** 3586–91
[21] Javey A, Guo J, Wang Q, Lundstrom M and Dai H 2003 Ballistic carbon nanotube field-effect transistors *Nature* **424** 654–7
[22] Woo Y, Duesberg G S and Roth S 2007 Reduced contact resistance between an individual single-walled carbon nanotube and a metal electrode by a local point annealing *Nanotechnology* **18** 095203
[23] Biswas C and Lee Y H 2011 Graphene versus carbon nanotubes in electronic devices *Adv. Funct. Mater.* **21** 3806–26
[24] Balandin A A, Ghosh S, Bao W, Calizo I, Teweldebrhan D, Miao F and Lau C N 2008 Superior thermal conductivity of single-layer graphene *Nano Lett.* **8** 902–7
[25] Giovannetti G, Khomyakov P A, Brocks G, Karpan V M, van den Brink J and Kelly P J 2008 Doping graphene with metal contacts *Phys. Rev. Lett.* **101** 026803
[26] Pei T, Xu H, Zhang Z, Wang Z, Liu Y, Li Y, Wang S and Peng L-M 2011 Electronic transport in single-walled carbon nanotube/graphene junction *Appl. Phys. Lett.* **99** 113102
[27] Kim W J, Lee J S, Lee S M, Song K Y, Chu C N and Kim Y H 2010 Better than 10 mA field emission from an isolated structure emitter of a metal oxide/CNT composite *ACS Nano* **5** 429–35
[28] Kerfriden S, Nahlé A H, Campbell S A, Walsh F C and Smith J R 1998 Short communication The electrochemical etching of tungsten STM tips *Electrochim. Acta* **43** 1939–44
[29] Chung M G, Kim D H, Lee H M, Kim T, Choi J H, Seo D K, Yoo J-B, Hong S-H, Kang T J and Kim Y H 2012 Highly sensitive NO2 gas sensor based on ozone treated graphene *Sensors Actuators* B **166–167** 172–6
[30] Lee S, Lee K and Zhong Z 2010 Wafer scale homogeneous bilayer graphene films by chemical vapor deposition *Nano Lett.* **10** 4702–7
[31] Lim S C, Jang J H, Bae D J, Han G H, Lee S, Yeo I-S and Lee Y H 2009 Contact resistance between metal and carbon nanotube interconnects: effect of work function and wettability *Appl. Phys. Lett.* **95**
[32] Lee S, Kahng S J and Kuk Y 2010 Nano-level wettings of platinum and palladium on single-walled carbon nanotubes *Chem. Phys. Lett.* **500** 82–5
[33] Zhang Y, Franklin N W, Chen R J and Dai H 2000 Metal coating on suspended carbon nanotubes and its implication to metal–tube interaction *Chem. Phys. Lett.* **331** 35–41
[34] Yang C, Hazeghi A, Takei K, Hong-Yu C, Chan P C H, Javey A and Wong H S P 2012 Low-resistance electrical contact to carbon nanotubes with graphitic interfacial layer *IEEE Trans. Electron Devices* **59** 12–9
[35] Yen M-Y, Hsiao M-C, Liao S-H, Liu P-I, Tsai H-M, Ma C-C M, Pu N-W and Ger M-D 2011 Preparation of graphene/multi-walled carbon nanotube hybrid and its use as photoanodes of dye-sensitized solar cells *Carbon* **49** 3597–606
[36] Huang J-H, Fang J-H, Liu C-C and Chu C-W 2011 Effective work function modulation of graphene/carbon nanotube composite films as transparent cathodes for organic optoelectronics *ACS Nano* **5** 6262–71
[37] Liang X *et al* 2011 Toward clean and crackless transfer of graphene *ACS Nano* **5** 9144–53
[38] Li X, Zhu Y, Cai W, Borysiak M, Han B, Chen D, Piner R D, Colombo L and Ruoff R S 2009 Transfer of large-area graphene films for high-performance transparent conductive electrodes *Nano Lett.* **9** 4359–63
[39] Sveningsson M, Hansen K, Svensson K, Olsson E and Campbell E E B 2005 Quantifying temperature-enhanced electron field emission from individual carbon nanotubes *Phys. Rev.* B **72** 085429
[40] Purcell S T, Vincent P, Journet C and Binh V T 2002 Hot nanotubes: stable heating of individual multiwall carbon nanotubes to 2000 K induced by the field-emission current *Phys. Rev. Lett.* **88** 105502
[41] Pan J Y, Zhu C C and Gao Y L 2008 Enhanced field emission characteristics of zinc oxide mixed carbon nano-tubes films *Appl. Surf. Sci.* **254** 3787–92